

Article

Using Moderate-Resolution Temporal NDVI Profiles for High-Resolution Crop Mapping in Years of Absent Ground Reference Data: A Case Study of Bole and Manas Counties in Xinjiang, China

Pengyu Hao ^{1,2,*}, Li Wang ^{1,*}, Yulin Zhan ¹ and Zheng Niu ¹

¹ The State Key Laboratory of Remote Sensing Science, Institute of Remote Sensing and Digital Earth, Chinese Academy of Sciences, CAS Olympic S & T Park, No. 20 Datun Road, P.O. Box 9718, Beijing 100101, China; zhanyl@radi.ac.cn (Y.Z.); niuzheng@radi.ac.cn (Z.N.)

² University of Chinese Academy of Sciences, No. 19A Yuquan Road, Beijing 100049, China

* Correspondence: haopy@radi.ac.cn (P.H.); wangli@radi.ac.cn (L.W.); Tel.: +86-137-1866-8296 (P.H.); +86-135-8190-3387 (L.W.)

Academic Editor: Wolfgang Kainz

Received: 15 March 2016; Accepted: 9 May 2016; Published: 16 May 2016

Abstract: Most methods used for crop classification rely on the ground-reference data of the same year, which leads to considerable financial and labor cost. In this study, we presented a method that can avoid the requirements of a large number of ground-reference data in the classification year. Firstly, we extracted the Normalized Difference Vegetation Index (NDVI) time series profiles of the dominant crops from MODIS data using the historical ground-reference data in multiple years (2006, 2007, 2009 and 2010). Artificial Antibody Network (ABNet) was then employed to build reference NDVI time series for each crop based on the historical NDVI profiles. Afterwards, images of Landsat and HJ were combined to obtain 30 m image time series with 15-day acquisition frequency in 2011. Next, the reference NDVI time series were transformed to Landsat/HJ NDVI time series using their linear model. Finally, the transformed reference NDVI profiles were used to identify the crop types in 2011 at 30 m spatial resolution. The result showed that the dominant crops could be identified with overall accuracy of 87.13% and 83.48% in Bole and Manas, respectively. In addition, the reference NDVI profiles generated from multiple years could achieve better classification accuracy than that from single year (such as only 2007). This is mainly because the reference knowledge from multiple years contains more growing conditions of the same crop. Generally, this approach showed potential to identify crops without using large number of ground-reference data at 30 m resolution.

Keywords: crop land mapping; reference NDVI time series; artificial antibody network; ground reference data; MODIS; Landsat/HJ

1. Introduction

Multi-temporal remote sensing data can be used to describe changes in vegetation characteristics over time [1–3], and these data have been employed to produce crop distributions from regional to national scales using both, supervised and unsupervised classifiers [4–10]. Moreover, the crop maps are the foundation for crop modeling, irrigation water distributions and land water management, which are important for decision makers [11–15]. However, most of the previous studies relied on the field reference data in the mapping year to train the classifiers [16,17]. When the cropland map need to be provided on yearly basis, the ground-reference data will be collected at annual frequency, which leads to considerable financial, time and labor costs [18]. In addition, national or local authorities do

not pay much attention to collecting ground-reference data sometimes, which lead to the difficulties in obtaining the ground reference data annually [19].

In areas with a stable cropping system, phenological metrics of the same specific crop are usually more similar than that of different crops among multi-years [18,20,21]. Thus, vegetation indices (VI), such as Normalized Difference Vegetation Index (NDVI) and Enhanced Vegetation Index (EVI), time series and the phenological metrics extracted from the VI time series have been used to transfer the knowledge of training samples from one year to another [21–25]. On the one hand, coarse spatial resolution data (such as Advanced Very High Resolution Radiometer, AVHRR and Moderate Resolution Imaging Spectroradiometer, MODIS), which are characterized by density temporal resolution, have shown the potential to identify crop types using the classification model built from the adjacent years [21], whereas a drawback is the relatively coarse spatial resolution cannot discriminate crop types in heterogeneous landscape [26–29]. Some pixel unmixing attempts, which are based on both linear and non-linear regression principles, have been proposed to solve this situation [30–33], but there are still some limitations: (1) the unmixing approaches can solely derive sub-pixel fractions of crop area in a pixel, and hardly provide the crop distribution within the pixel; (2) the VI profiles of some crops maybe too similar to be reliably separated; and (3) if the endmembers were extracted across multiple years, the inter-annual differences will result in the variable temporal signatures of endmembers of the same crop [30].

On the other hand, the image time series at finer spatial resolution, such as Landsat Thematic Mapper (TM) and Satellite Pour l'Observation de la Terre (SPOT), have shown the potential to discriminate crops [5,15,34]. Note that there have been some attempts at identifying crop types without ground reference data of the classification year using the spectrum at specific phenological periods [22,23]. The limitation of these methods is that they have to extract phenological metrics using high resolution image time series (such as Landsat) in the classification year, which result in the difficulty of the application of these methods in large area for the following reasons: (1) within one year, it is difficult to obtain cloud-free image time series that are dense enough to extract phenological metrics in large areas by a single sensor (such as Landsat 5); and (2) although the temporal resolution of the image time series can be improved by combining the data from multi-sensor [35,36], the radiometric differences among different sensors may have negative influence on the accuracy of the phenological metrics [37].

The objective of this study is to propose a method and classify crop types at high resolution (30 m) without the use of the ground reference samples in the classification year. To achieve this purpose, we combined the advantages of both moderate resolution (MODIS) and high resolution (Landsat and Huan Jing) data. First, we acquired the historical ground reference data of multiple years (2006, 2007, 2009 and 2010); the NDVI profiles of the crops were extracted from MODIS NDVI time series using historical ground reference data; and reference NDVI time series were then obtained from the historical NDVI profiles. Afterwards, the linear relations between Landsat/HJ NDVI and MODIS NDVI during the entire crop-growing season were obtained, and the reference NDVI time series were transformed using the linear relations. Finally, the transformed reference NDVI time series were utilized to identify crop types at 30 m resolution.

2. Study Regions and Data Description

2.1. Description of the Study Area and the Crop Calendar

In this study, we selected two representative agricultural regions in northern Xinjiang, Bole County and Manas County. Bole County ($44^{\circ}20' \sim 45^{\circ}23'N$, $80^{\circ}40' \sim 82^{\circ}42'E$) covers 32 kha of cropland (Figure 1a), and the average temperature and rainfall is $14.1^{\circ}C$ and 144.4 mm during the crop period (between April and October), respectively. Manas County ($43^{\circ}17' \sim 45^{\circ}20'N$, $85^{\circ}17' \sim 86^{\circ}46'E$) covers 180 kha of cropland (Figure 1a), the average temperature and rainfall are $14.4^{\circ}C$ and 153.2 mm during the crop period, respectively.

Cropland covers 13.7% (more than 1100 ha) and 15.8% (more than 1800 ha) of the total area in Bole and Manas, respectively. The dominant crops grown in the study areas include cotton, spring maize, watermelon, grape, tomato, and wheat. The vegetation cover fraction for each crop type over the course of a year is presented in Figure 1b. Cotton, spring maize, watermelon, tomato, and grape are planted in early April and begin their growth mostly during the June–July period. Watermelon and tomato are harvested in August, spring maize is harvested in early September, and grape and cotton are harvested during the August–September and September–October periods, respectively. However, the field for winter wheat is a bit complex. Winter wheat is planted in early November, begins its growth in the next April, and is reaped for harvest in late June. After the harvest, some fields are in rotation, and others are used to plant some other summer crops, mainly summer maize. Hence, we divided the winter wheat into two parts relying on whether summer crops are planted in the same field or not.

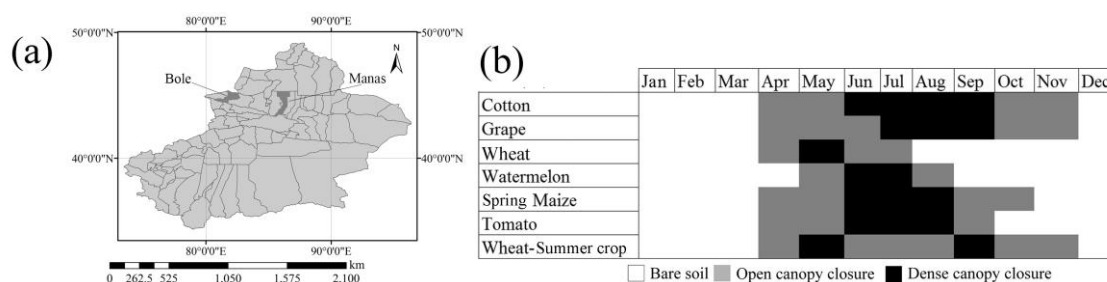


Figure 1. (a) The extent of Xinjiang and the locations of the study areas of this study; and (b) vegetation cover fractions for different crop types over the course of a year.

2.2. Datasets

2.2.1. MODIS Imagery

Sixteen-day composite Terra MODIS 250m NDVI data from the MOD13Q1 Vegetation Indices product were used in this study. These data were downloaded from Land Processes Distributed Active Archive Centre [38], and two MODIS tiles (h23v04 and h24v04) were used to cover all of the field sites. The MODIS NDVI images are consisted of 15 scenes (21 March–1 November) in each year and spanned five crop years (2006, 2007 and 2009–2011). The MODIS images were mosaicked and re-projected from Sinusoidal to UTM WGS84 zone 44N (Bole) and zone 45N (Manas).

2.2.2. TM and HJ-CCD Imagery

Images used in this study are listed in Tables 1 and 2. Data from both Landsat TM/ETM+ and Huan Jing (HJ) CCD with cloud-cover of less than 10% were used to acquire the time series at 30 m spatial resolution. The HJ-1 Constellation has two satellites (HJ-1A and HJ-1B), and each satellite had two CCD cameras. Compared with Landsat TM images, HJ data have similar spatial resolution (30 m), and finer temporal resolution (four days). Table 3 shows the spectral range of Landsat-5 TM and HJ-1 CCD in Red and Near-Infrared (NIR) bands, which were used to calculate NDVI.

Table 1. The dates of Landsat TM/ETM+ and HJ images (in Bole).

Year	Sensor	April	May	June	July	August	September	October
2006	TM ETM+	16th			29th			1st
2007	TM		29th			1st	2nd	
2009	TM			19th	21st		24th	
2010	TM		5th		8th		26th	
2011	TM	6th, 22nd	24th		11st, 27th		13th 27th	
	HJ1A-CCD1							
	HJ1A-CCD2 HJ1B-CCD1		10th			16th		16th

Table 2. The dates of Landsat TM/ETM+ and HJ CCD images (in Manas).

Year	Sensor	April	May	June	July	August	September	October
2006	TM ETM+		20th		31st		17th	
2007	TM		15th		2nd		4th	
2009	TM		20th		7th		5th	
2010	TM			8th		11th		14th
2011	TM	24th	10th	28th	13th, 29th			1st 15th, 27th
	HJ1A-CCD2						16th	
	HJ1B-CCD1 HJ1B-CCD2		28th			15th		

Notes: Images in 2006, 2007, 2009 and 2010 were used to obtain field boundary, and images in 2011 were used to classify crops.

Table 3. Red and NIR bands of Landsat-5 TM and HJ-1 CCD.

Landsat-5 TM Spectral Bands		HJ-1 CCD Spectral Bands
#	Band width (μm)	Band width (μm)
3	0.630–0.690 (Red)	0.63–0.69 (Red)
4	0.775–0.900 (NIR)	0.76–0.90 (NIR)

The Landsat-5 TM surface reflectance product (CDR) and the HJ Level 2 standard product (DN value) were used to classify crop types in 2011 at 30 m resolution in this study [39,40]. Images were georeferenced to the UTM WGS 84 zones 44N (Bole county) and 45N (Manas county). The HJ images were registered to the TM images, achieving a RMSE of less than 0.3 pixels using a 2nd order polynomial transformation and bi-linear resampling. Subsequently, radiance calibration and FLAASH atmospheric correction were performed for HJ-1 CCD images [41]. Normalized Difference Vegetation Index (NDVI) time series was employed in this study, and we used Red and NIR bands to calculate NDVI (Equation (1)).

$$NDVI = \frac{\rho(NIR) - \rho(Red)}{\rho(NIR) + \rho(Red)} \quad (1)$$

where $\rho(NIR)$ and $\rho(Red)$ were the land surface reflectance of the NIR band (0.775~0.9 μm) and Red band (0.63~0.69 μm), respectively. As for the Landsat-5/7 data during 2006 and 2010, we used the original images with DN value because these images were just utilized to identify crop fields containing entire MODIS pixels.

2.2.3. Ground-Reference Data

In this study, the ground-reference data were divided into two parts: historical field samples used for building reference NDVI time series across four years (2006, 2007, 2009 and 2010), and field samples used for validating classification accuracy in 2011. The distribution of the ground reference data is shown in Figure 2.

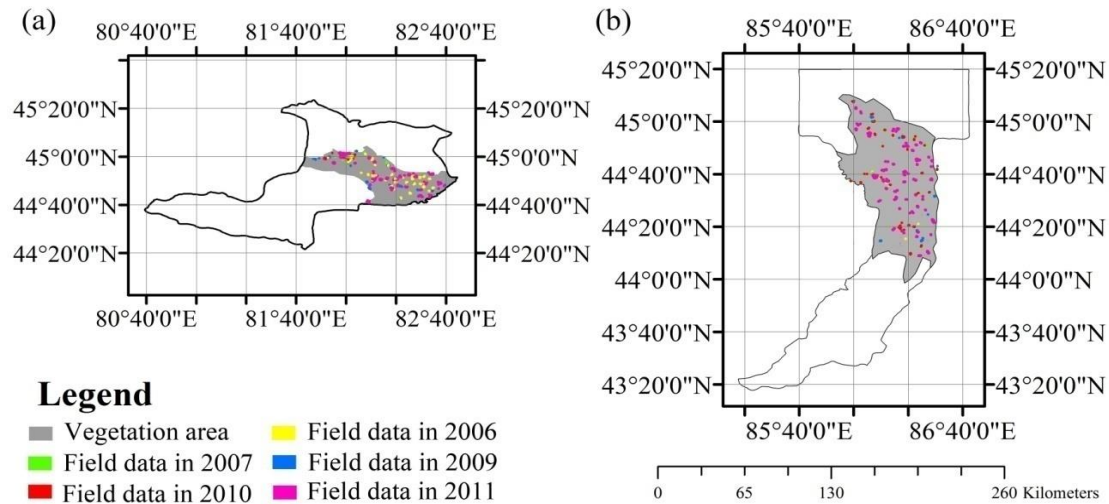


Figure 2. Distributions of ground reference data: (a) Bole; and (b) Manas.

To obtain the historical field samples, we selected 33 and 30 sampling frames (1 km by 1 km) in Bole and Manas, respectively. Then, NDVI of all Landsat images during 2006 and 2011 were calculated, and the field boundaries were visually interpreted in each sampling frame based on the 30 m NDVI images of each year. Afterwards, the field boundaries were overlaid on the MODIS images, and the fields that did not contain entire MODIS pixels were removed. The crop type information during 2006 and 2010 of the remained fields was obtained from the local statics Bureau and farmers during the field survey work in 2011. Subsequently the historical NDVI time series were extracted from pure ground reference MODIS pixels. If there were more than 13 “good data” periods in a reference pixel among the “Pixel Reliability” of the 15 time periods [38], the pixel was retained. Otherwise, the pixel was removed from the historical reference dataset. For the remaining pixels, the NDVI for low-quality periods (if the quality of a pixel is not “good data”, we define it as “low-quality”) was replaced by the average NDVI of the previous and following periods. Finally, there were 1061 samples of the seven major crop types in the study area in total (Table 4). We did not collect the historical field samples in 2008 because we did not obtain Landsat-5 TM images in 2008 before our field survey. Thus, the crop types of 2008 were not retrieved during the farmer interview. The procedure for obtaining the historical ground reference samples is shown in Figure 3.

Table 4. The number of historical samples (pixels at 250 m) by year and crop type.

Crop	2006	2007	2009	2010	Total
Cotton	177	219	239	157	792
Spring Maize	14	13	21	6	54
Grape	12	15	34	20	81
Wheat	21	8	23	10	62
Wheat-Summer Crop	3	5	9	7	24
Watermelon	10	6	2	4	22
Tomato	0	0	17	9	26
Total	237	266	345	213	1061

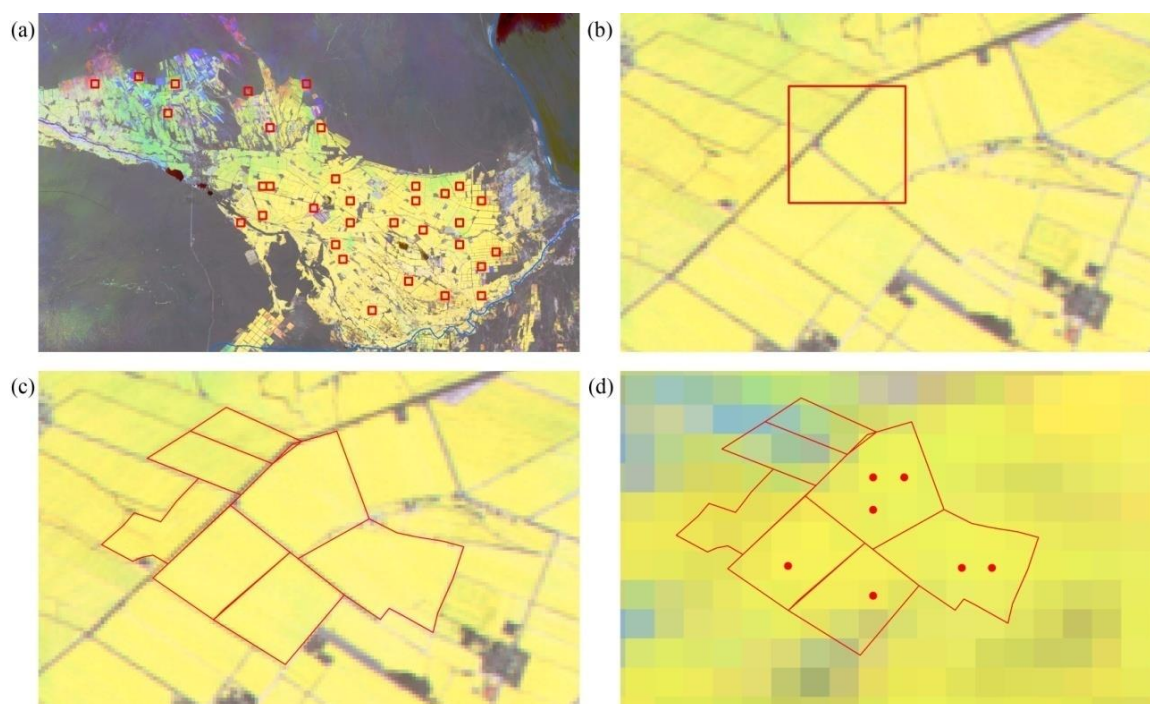


Figure 3. Procedure of collecting the historical reference data: (a) The distribution of sampling frames; (b) one of the 1 km by 1 km frames; (c) crop field boundaries of a frame; and (d) select MODIS pixels that could be used as ground reference sample. The images in the figure are composed of R: NDVI of Landsat TM image (29 May 2007), G: NDVI of Landsat TM image (1 August 2007), and B: NDVI of Landsat TM image (2 September 2007).

The validation field samples were collected by field research of the study area during 2011. These field samples were selected to represent the full variety of crop types and an even distribution across the study areas. A total of 525 fields in Bole and 463 fields in Manas were selected and surveyed. For each field, the crop type was collected as attribute information. Field boundaries were recorded using GPS, and digitized as polygons. All polygons were converted to raster format using the TM grid (30 m spatial resolution), and boundary pixels were removed to ensure that all samples are pure crop pixels. In addition, the polygons were overlaid on the MODIS grid (250 m resolution), and the MODIS pure pixels were obtained. To compare the results derived from historical reference with that derived from the ground-reference data, some of the samples were used as training samples. The number of training and validation samples is shown in Table 5.

Table 5. The number of training and validation samples in 2011.

	Bole			Manas		
	Surveyed Fields (Polygons)	Training (Pixels at 30 m)	Validation	Surveyed Fields (Polygons)	Training (Pixels at 30 m)	Validation
Cotton	229	500	4542	269	350	4081
Spring Maize	36	150	699	63	300	1674
Grape	43	300	1169	0	0	0
Wheat	74	350	1038	54	300	1468
Wheat-Summer Crop	68	200	840	28	50	434
Watermelon	75	350	1044	0	0	0
Tomato	0	0	0	49	150	1277
Total	525	1850	9332	463	1150	8843

3. Methods

The methodology of the study was presented in Figure 4. This study was composed of six main parts: (1) extracting NDVI time series profiles from MODIS data using ground reference data in 2006, 2007, 2009 and 2010; (2) building historical reference NDVI time series (between 2006 and 2010) for each crop using ABNet based on the historical NDVI time series profiles, and measuring the separability of reference NDVI for crop classification; (3) using Landsat-5 TM and HJ data to build multi-source NDVI time series at 30 m resolution in 2011; (4) testing the linear relationship between Landsat/HJ and MODIS NDVI, and then transforming the reference NDVI time series using the linear relation; (5) using the transformed reference time series to classify crop types at 30 m spatial resolution; and (6) assessing classification accuracy. Additionally, the classification accuracy was compared with the result derived from ground-reference data of 2011.

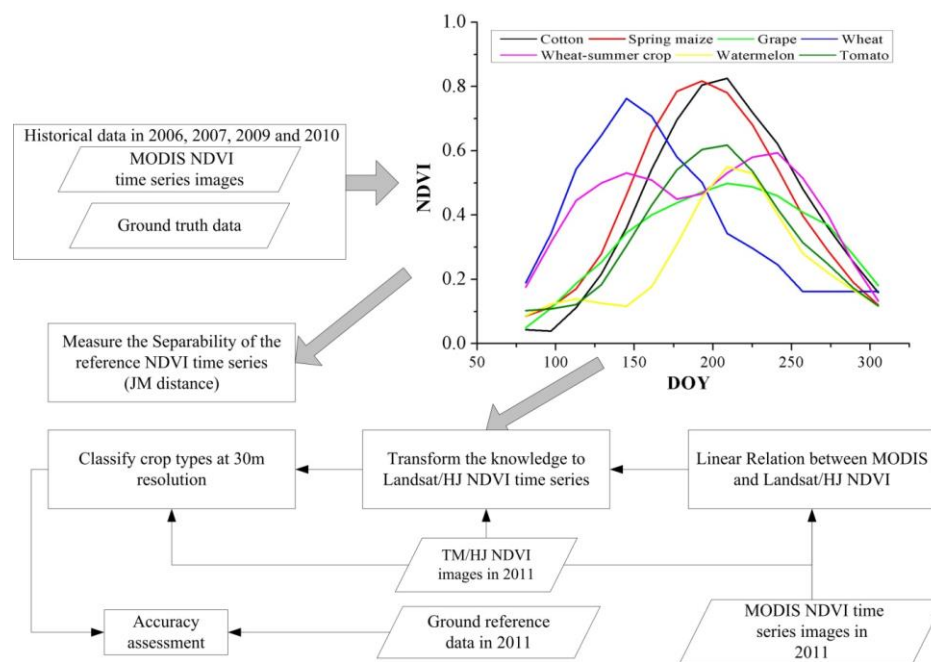


Figure 4. Study methodology.

3.1. Artificial Antibody Network

The Artificial Antibody Network (ABNet) was proposed by Zhong and Zhang [42] based on artificial immune network principles (AIN). The antibody model was used as the basic component for the ABNet and each antibody contained three attributes: the crop type of the antibody, center vector and the recognizing radius. The ABNet have two procedures: training and classification. During the training procedure, the training antigens were used as input of the ABNet, and the antibodies were obtained. Then, in the classification procedure, the antibodies were used to identify new antigens.

The training procedure of the ABNet contained five steps for each class: pre-selection, cloning, mutation, adaptive calculation of new antibodies and antibody reorganization. The detailed training process can be found in work of Zhong and Zhang [42]. While training the ABNet, an important issue was to select a similarity measure, and we used Euclidean distance (Equation (2)) [43], which can easily measure the similarity in the training process:

$$ED(a, b) = \sqrt{\sum_{t=1}^n (a_t - b_t)^2} \quad (2)$$

where a_t and b_t are the values of time series a and b at moment t , respective, and N is the number of samples in the time series. Moreover, the ABNet can build up a network and guarantee its convergence adaptively, and no more parameters need further optimized.

The classification procedure was to calculate the Euclidean distance between vector of a new antigen and the center vector of each antibody, and the new antigen was labeled as the crop type of the antibody with the minimum distance if the minimum distance was less than the recognizing radius of the antibody. Otherwise, the spectral angle (Equation (3)) was calculated between the vector of the new antigen and the center vector of the antibodies [44], and the antigen was labeled as the crop type of antibody with the minimum spectral angle.

$$\text{SAM}(a, b) = \cos^{-1} \left(\frac{\sum_{t=1}^n (a_t \cdot b_t)}{\sqrt{\sum_{t=1}^n (a_t)^2} \sqrt{\sum_{t=1}^n (b_t)^2}} \right) \quad (3)$$

We employed ABNet in this study to build the reference NDVI time series for each crop because ABNet can adaptively build up the network and guarantee its convergence without any parameters. In addition, one crop type can contain many antibodies, and the ABNet could recognize different distinctive patterns that are suitable for identifying the same crop in different situations with variable NDVI time series. In this study, the ABNet was interpreted in IDL.

3.2. Building the Reference NDVI Time Series for the Crops

We used the ABNet to build the reference NDVI time series. First, we extracted the NDVI time series from the ground reference samples of both Bole and Manas. Then, all historical NDVI profiles were used as input of the ABNet training process, and the antibodies were then obtained. The center vectors of the antibodies were the reference NDVI time series for each crop type, and multiple reference NDVI time series profiles were obtained to describe the same crop under different conditions.

3.3. Measuring the Separability of Reference NDVI Time Series

In this study, we used the Jeffries-Matusita (JM) distance to measure the separability of the reference NDVI time series for each pair of crops because previous studies showed that JM distance could better measure the separability among different classes than other distances, such as Euclidean distance or divergence [41,45]. The JM distance between a pair of class and specific functions was given by:

$$\text{JM}(c_i, c_j) = \int_x \left(\sqrt{p(x|c_i)} - \sqrt{p(x|c_j)} \right)^2 dx \quad (4)$$

where x denotes a span of VI time series values and c_i and c_j (lowercase c) denote the two crop classes under consideration. Under normality assumptions, Equation (2) was reduced to $\text{JM} = 2(1 - e^{-B})$, where:

$$B = \frac{1}{8} (\mu_i - \mu_j)^T \left(\frac{C_i + C_j}{2} \right)^{-1} (\mu_i - \mu_j) + \frac{1}{2} \ln \left(\left| \frac{|C_i + C_j|}{2\sqrt{|C_i| \times |C_j|}} \right| \right) \quad (5)$$

and C_i and C_j (uppercase C) are the covariance matrixes of class i and j , respectively. Additionally, $|C_i|$ and $|C_j|$ are the determinants of C_i and C_j , respectively. The JM distance ranged from 0 to 2, with a large value indicating a high level of separability between two classes [46].

3.4. Testing the Relation between MODIS and Landsat/HJ NDVI

We combined the Landsat-5 TM and HJ-1 NDVI in 2011 to increase the temporal resolution of NDVI time series at 30 m resolution. For each Landsat TM/HJ CCD NDVI image, we selected the MODIS image whose temporal flag is the nearest to the date that Landsat TM/HJ CCD images were

acquired. When testing the relationship between Landsat TM/HJ CCD NDVI and MODIS NDVI, the samples were selected in homogenous crop fields, and the average NDVI of all Landsat TM/HJ CCD pixels to the corresponding MODIS pixel were calculated. Coinciding with some previous studies, Landsat TM/HJ CCD NDVI and MODIS NDVI showed strong linear relationships ($R^2 > 0.8$ in Figures 5 and 6) [37,47,48]. Then, all reference NDVI time series were transformed to Landsat/HJ NDVI using corresponding linear relation, and the transformed reference NDVI time series were used to identifying crop types in the next step.

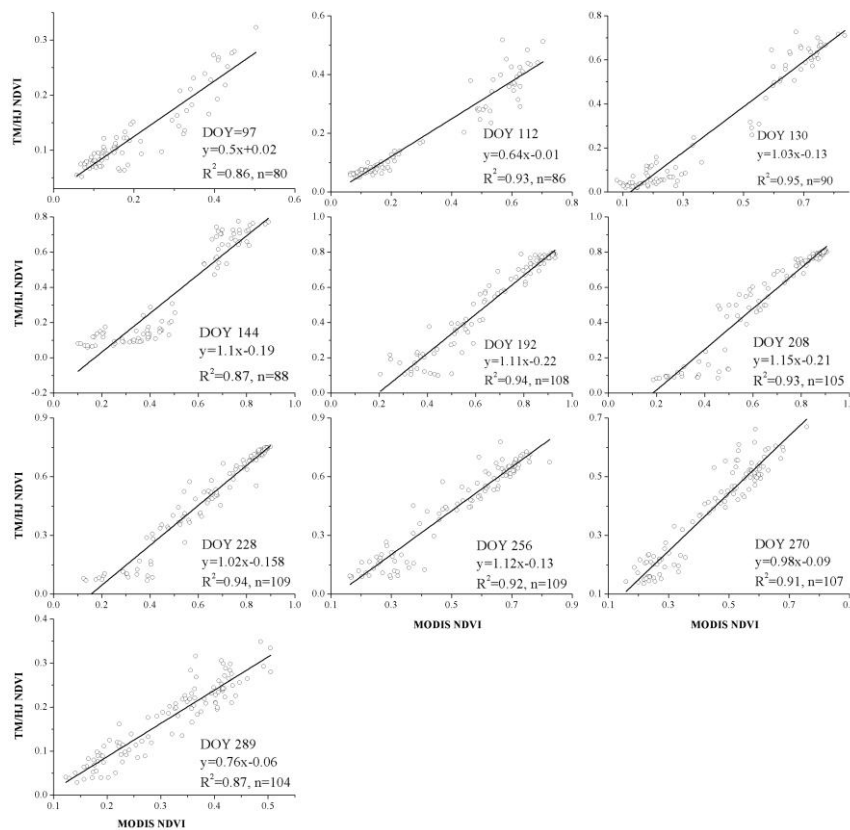


Figure 5. The relationship between the TM/HJ-CCD (NDVI calculated from the TM/HJ images) and the MODIS NDVI (NDVI calculated from the MODIS images) during the growing season for crops in Bole County during 2011. DOY, day of year; n, the number of samples used for the transformation.

3.5. Crop Classification at 30 m Resolution

We first masked the non-agricultural area using the “agriculture land” of Finer Resolution Observation and Monitoring of Global Land Cover (FROM-GLC) at 30 m spatial resolution [49]. Before the masking, we randomly selected 300 validation pixels in both study regions using Hawth's Tools [50]; all validation samples were visually interpreted as crop/non-crop (Table 6), and these validation samples were used to verify the accuracy of the crop mask. The overall accuracies were above 90% for both study areas, which indicated that the crop mask of both study regions were accurate enough to mask non-crop area. Next, we classified the crops at 30 m resolution using the transformed reference NDVI time series by the classification procedure of ABNet. In addition, we used a portion of the ground-reference data as training samples to classify the agricultural area for comparison. The classifier was also ABNet.

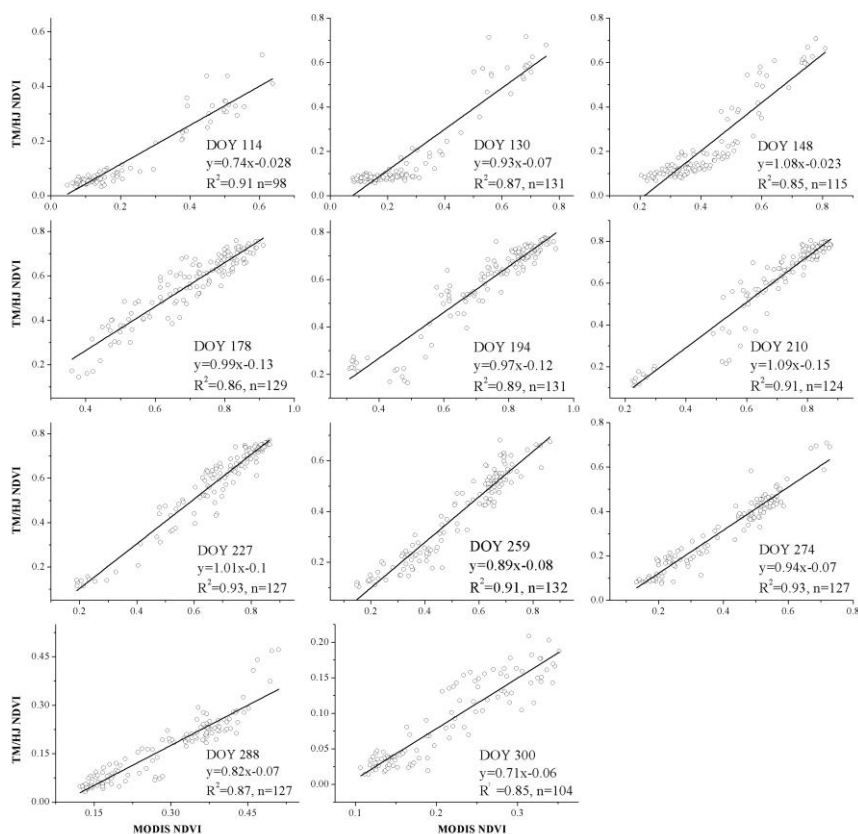


Figure 6. The relationship between the TM/HJ-CCD (NDVI calculated from the TM/HJ images) and the MODIS NDVI (NDVI calculated from the MODIS images) during the growing season for crops in Manas County during 2011 ($n = 345$). DOY, day of year; n , the number of samples used for the transformation.

Table 6. Confusion-matrix of the classification process of “crop” and “non-crop” (%).

	Bole		Manas	
	Non-Crop	Crop	Non-Crop	Crop
PA	87.39	97.88	88.39	95.17
UA	96.04	92.96	95.14	88.46
OA	90.67		91.67	

Note: UA, user’s accuracy; PA, producer’s accuracy; OA, Overall accuracy.

4. Results

4.1. Reference NDVI Time Series

For each crop type, the reference NDVI time series were plotted in Figure 7. Among the summer crops, cotton was the major crop type in the study region, and had the largest amount of reference NDVI time series among all crops. The highest NDVI value of cotton was between 0.75 and 0.9 around Day 190 (late July). For spring maize, the highest value was similar to cotton, but after the peak, NDVI of spring maize decreased faster than cotton, and at around Day 250 (September), NDVI of spring maize was relatively lower than cotton. Tomato also had the highest NDVI around Day 190, but the NDVI value was between 0.5 and 0.6, which was significantly lower than cotton and spring maize. For grape, NDVI was high during Days 170–250 (from late June to early September). In addition, the variability of grape was the largest among all crops in the study region (between 0.4 and 0.7). Another summer crop was watermelon, which had a relatively short growing season, with NDVI peak

at around Day 210 (late July). The major winter crop in the study areas was winter wheat, the time period of high NDVI (above 0.5) value was between Days 120 and 130. After the harvest of the winter wheat, some fields were used to plant the summer crops. The crops were sown at about Day 200 and then reach NDVI peak between Days 230 and 270. As there are various crop types, the NDVI profile differed, while we did not identify the summer crop types and just labeled all pixels with a NDVI peak after the harvest of wheat as wheat-summer crop.

Period-by-period JM distances were calculated using the reference NDVI time series of different crop types. The result (Figure 8) showed that the winter wheat and wheat-summer crop can be distinguished from the other crops between day 120 and 140 with the early NDVI peak. In addition, wheat could be discriminated from wheat-summer crop at day 170 because of the development of the summer crops. Grape had the lowest separability among all crops, and the average JM distance between grape and all other crops were around 0.5 in each time period. This was attributed to the large variability of the reference NDVI time series of grape. For example, some grape reference profiles had low NDVI, but some other grape reference time series had high NDVI values, which were similar to the cotton profiles. Moreover, cotton and spring maize had relatively low separability (1.994 in Table 7) because of the similar NDVI during the majority of the growing season (between Days 81 and 225 in Figure 8), and the similarity between cotton and spring maize was also observed by [51,52] in Uzbekistan. Generally, JM distances for all pair-wise crop comparisons were above 1.9 when all time periods in the entire growing season were used (Table 7), which indicated that the reference NDVI time series of each crop was separable in the study region.

Table 7. JM distances for all pair-wise crop comparisons during the entire time series.

	Spring Maize	Grape	Wheat	Wheat-Summer Crop	Watermelon	Tomato
Cotton	1.994	1.997	2.000	2.000	2.000	2.000
Spring maize		2.000	2.000	2.000	2.000	1.998
Grape			2.000	2.000	2.000	2.000
Wheat				2.000	2.000	2.000
Wheat-Summer Crop					2.000	2.000
Watermelon						2.000

4.2. Classification Accuracy Assessment

The results of the accuracy assessment (overall accuracy, Kappa coefficient, user's and producer's accuracy) for the two study areas are summarized in Tables 8 and 9 [53,54]. If the historical NDVI time series of single year is used to build the reference NDVI profiles, the classification accuracies were low. For example, when the historical NDVI time series of 2007 were used to build the reference NDVI time series, the overall accuracy was 73.01%. The summer crops, such as spring maize, watermelon and grape were seriously mislabeled as cotton. Moreover, the reference tomato NDVI time series were not collected in 2006 and 2007; as a result, the reference profiles obtained from only 2006 and 2007 cannot identify tomato in 2011.

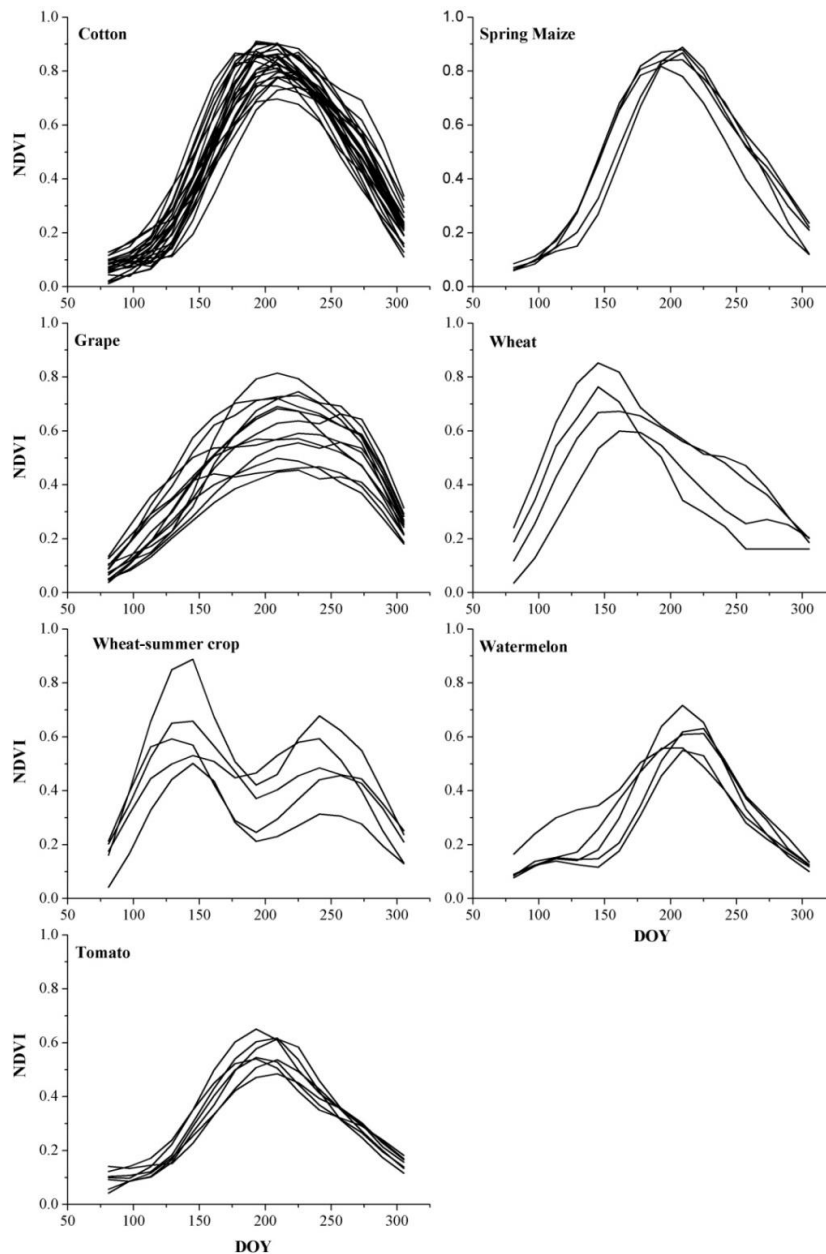


Figure 7. Reference NDVI time series for crops in the study area.

When the historical NDVI time series among 2006 and 2010 were used to build the reference time series, the classification accuracy improved significantly. The overall accuracy in Bole and Manas were 87.13% and 83.48%, respectively, which were acceptable for crop mapping without the use of ground reference data in the classification year. In Bole, both producer's and user's accuracy (PA and UA) of cotton, watermelon, wheat and wheat-summer crop were above 80%; but PA and UA of grape were about 70% because cotton and grape were confused: 280 cotton pixels were mislabeled as grape, while 260 grape pixels were wrongly classified as cotton. Spring maize had low UA (70.16%) because more than 200 cotton pixels were labeled as spring maize. In Manas, PA of cotton, spring maize, wheat and wheat-summer crop were higher than 80%, but the UA of spring maize and wheat were low (only 71.54% and 65.43%, respectively) because 272 and cotton samples were mislabeled as spring maize and wheat, respectively.

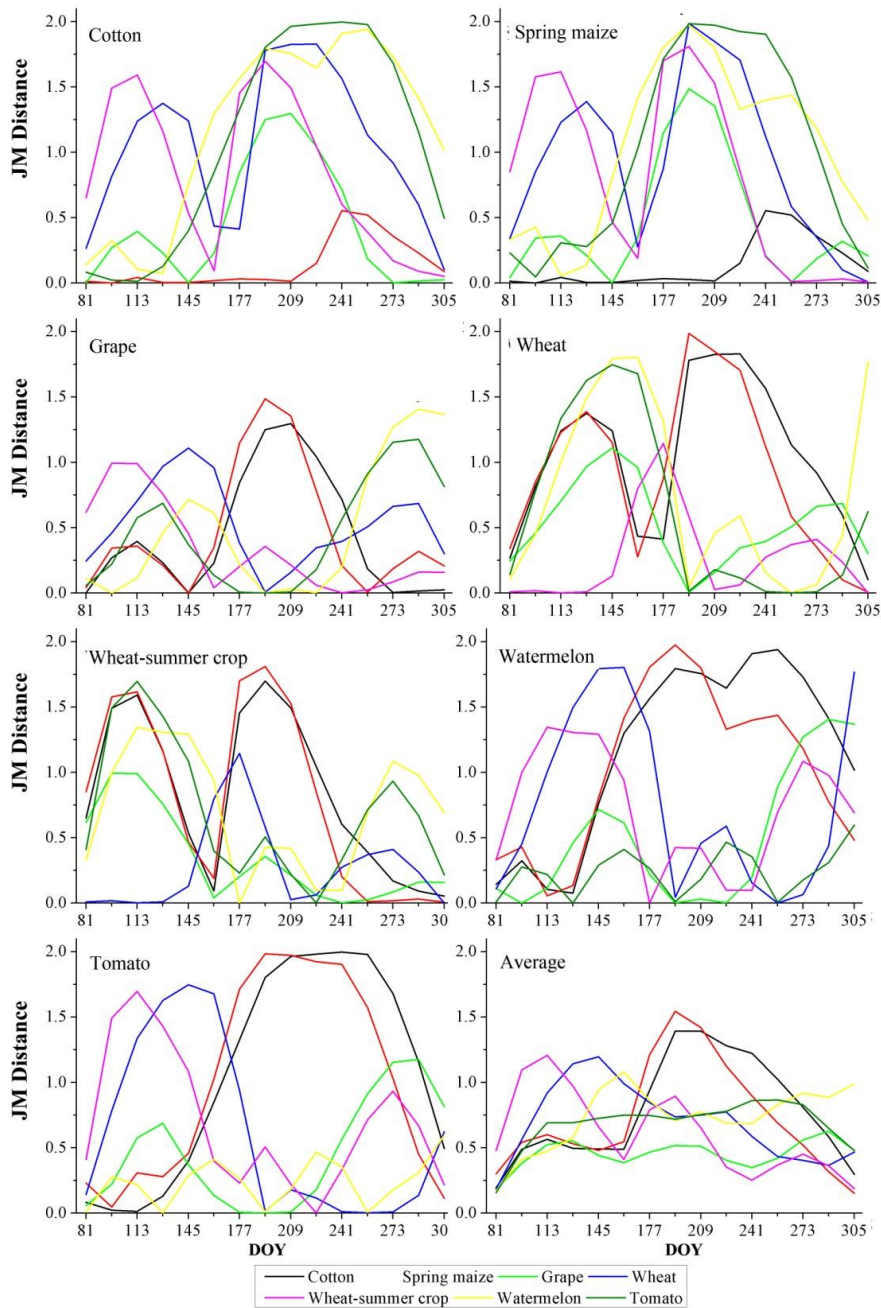


Figure 8. JM distances of all pair-wise crop comparisons for reference NDVI time series.

To assess the quality of the classification process based on the historical reference NDVI time series, a portion of the ground-reference data were used to classify the crops using the same classifier (ABNet). The overall accuracies for Bole and Manas were found to be 90.21% and 86.87%, respectively, which were higher compared to the accuracies for the historical reference NDVI-derived classification. In Bole, the increase of the accuracy was mainly caused by the better identification of wheat and wheat-summer crop (both PA and UA of wheat and wheat-summer crop were higher than 98%). In Manas, more correctly classified cotton and tomato pixels contributed to the improvement of the overall accuracy.

Table 8. Error matrix for Bole.

Ground Truth Data							
	Cotton	Spring Maize	Grape	Wheat	Wheat-Summer Crop	Watermelon	UA (%)
Using reference sample of 2006, OA = 78.63%, Kappa = 0.67							
Cotton	4208	516	485	0	0	461	74.22%
Spring Maize	8	183	30	11	0	287	35.26%
Grape	45	0	626	1	8	61	84.48%
Wheat	0	0	0	1000	14	0	98.62%
Wheat-Summer Crop	0	0	0	0	858	0	100.00%
Watermelon	0	0	5	0	0	234	97.91%
PA (%)	98.76%	26.18%	54.62%	98.81%	97.50%	22.44%	
Using reference sample of 2007, OA = 73.01%, Kappa = 0.59							
Cotton	4166	118	660	11	0	611	74.85%
Spring Maize	1	278	0	0	0	0	99.64%
Grape	3	0	54	0	12	0	78.26%
Wheat	0	0	0	803	0	0	100.00%
Wheat-Summer Crop	6	0	195	197	868	0	68.56%
Watermelon	85	303	237	1	0	432	40.83%
PA (%)	97.77%	39.77%	4.71%	79.35%	98.64%	41.42%	
Using reference sample of 2009, OA = 78.95%, kappa = 0.68							
Cotton	4240	523	664	9	0	509	71.32%
Spring Maize	0	176	10	2	0	140	53.66%
Grape	21	0	464	0	9	3	93.36%
Wheat	0	0	0	996	0	0	100.00%
Wheat-Summer Crop	0	0	0	4	871	0	99.54%
Watermelon	0	0	8	1	0	391	97.75%
PA (%)	99.51%	25.18%	40.49%	98.42%	98.98%	37.49%	
Using reference sample of 2010, OA = 82.96%, Kappa = 0.76							
Cotton	3763	183	385	9	0	283	81.40%
Spring Maize	207	516	15	0	0	62	64.50%
Grape	285	0	736	0	0	0	72.09%
Wheat	0	0	0	953	46	0	95.40%
Wheat-Summer Crop	0	0	0	47	834	0	94.67%
Watermelon	6	0	10	3	0	698	97.35%
PA (%)	88.31%	73.82%	64.22%	94.17%	94.77%	66.92%	
Using reference sample of 2006~2010, OA = 87.13%, Kappa = 0.82							
Cotton	3747	11	260	0	0	0	93.26%
Spring Maize	221	623	10	0	0	34	70.16%
Grape	280	0	821	0	1	40	71.89%
Wheat	0	0	0	909	71	0	92.76%
Wheat-Summer Crop	0	0	0	91	808	0	89.88%
Watermelon	13	65	55	12	0	969	86.98%
PA (%)	87.94%	89.13%	71.64%	89.82%	91.82%	92.91%	
Using ground reference data, OA = 90.21%, Kappa = 0.87							
Cotton	3752	0	44	0	0	0	98.84%
Spring Maize	78	665	7	0	0	53	82.81%
Grape	379	0	870	0	0	0	69.66%
Wheat	0	0	0	1000	1	0	99.90%
Wheat-Summer Crop	0	0	0	0	879	0	100.00%
Watermelon	52	34	225	12	0	990	75.40%
PA (%)	88.05%	95.14%	75.92%	98.81%	99.89%	94.92%	

Note: UA, user's accuracy; PA, producer's accuracy.

Table 9. Error matrix for Manas.

Ground Truth Data						
	Cotton	Spring Maize	Wheat	Wheat-Summer Crop	Tomato	UA (%)
Using reference sample of 2006, OA = 79.71%, Kappa = 0.69						
Cotton	3288	178	61	0	-	93.22%
Spring Maize	791	1365	225	0	-	57.33%
Wheat	0	131	1071	56	-	85.14%
Wheat-Summer Crop	0	0	110	378	-	77.18%
PA (%)	80.61%	81.54%	73.01%	86.92%	-	
Using reference sample of 2007, OA = 67.08%, Kappa = 0.41						
Cotton	3990	1657	325	0	-	66.81%
Spring Maize	89	17	58	5	-	10.06%
Wheat	0	0	700	0	-	100.00%
Wheat-Summer Crop	0	0	384	429	-	52.42%
PA (%)	97.82%	1.02%	47.72%	98.83%	-	
Using reference sample of 2009, OA = 79.24%, Kappa = 0.71						
Cotton	3858	101	2	0	9	97.18%
Spring Maize	145	861	285	0	372	51.77%
Wheat	0	0	1041	12	0	98.86%
Wheat-Summer Crop	0	0	15	422	0	96.52%
Tomato	76	712	124	0	896	49.56%
PA (%)	94.58%	51.43%	70.96%	97.20%	70.16%	
Using reference sample of 2010, OA = 67.75%, Kappa = 0.57						
Cotton	3135	0	2	0	0	99.94%
Spring Maize	879	185	1	0	1	17.35%
Wheat	0	0	1023	0	0	100.00%
Wheat-Summer Crop	0	0	42	434	0	91.06%
Tomato	65	1489	399	0	1276	39.52%
PA (%)	76.86%	11.05%	69.73%	100.00%	99.92%	
Using reference sample of 2006~2010, OA = 83.48%, Kappa = 0.77						
Cotton	3525	17	1	0	0	99.44%
Spring Maize	272	1423	74	0	220	71.54%
Wheat	269	185	1200	53	127	65.43%
Wheat-Summer Crop	0	0	153	381	0	71.02%
Tomato	13	49	39	0	928	90.18%
PA (%)	86.42%	85.01%	81.80%	87.62%	72.67%	
Using ground reference data, OA = 86.87%, Kappa = 0.82						
Cotton	3662	2	0	7	0	99.75%
Spring Maize	227	1485	4	0	137	80.14%
Wheat	0	0	1054	1	0	99.91%
Wheat-Summer Crop	0	0	0	417	0	100.00%
Tomato	190	187	409	9	1140	58.91%
PA (%)	89.78%	88.71%	71.85%	96.08%	89.27%	

Note: UA, user's accuracy; PA, producer's accuracy. In addition, as the ground reference sample of tomato was not acquired in 2006 and 2007, so that the classification using 2006/2007 samples did not include tomato.

Figure 9 shows the crop map in Bole and Manas for year 2011. Cotton was the major crop type in both study areas, comprising 67.79% and 62.68% of cropland in Bole and Manas, respectively. In Bole, cotton was mainly distributed in the central county, and spring maize was mainly planted in the northwest of the county. Other crops, such as grape and watermelon were planted in the northern

county. In Manas, cotton was mainly planted in the central and northern counties; and spring maize was planted in the southern county. As the crop identification were conducted at pixel level, there were some inter-field misclassifications, which was mainly due to the crop situation variation. In addition, the field boundaries were always misclassified. This was mainly because the boundary pixels were always mixed pixels combining crops and the road beside the crop fields. The mixed NDVI signature was perhaps more similar to the NDVI of a different crop, which led to the misclassification. As the training and validation samples did not contain field boundary pixels, these misclassification were not reported in the accuracy assessment confusion matrix.

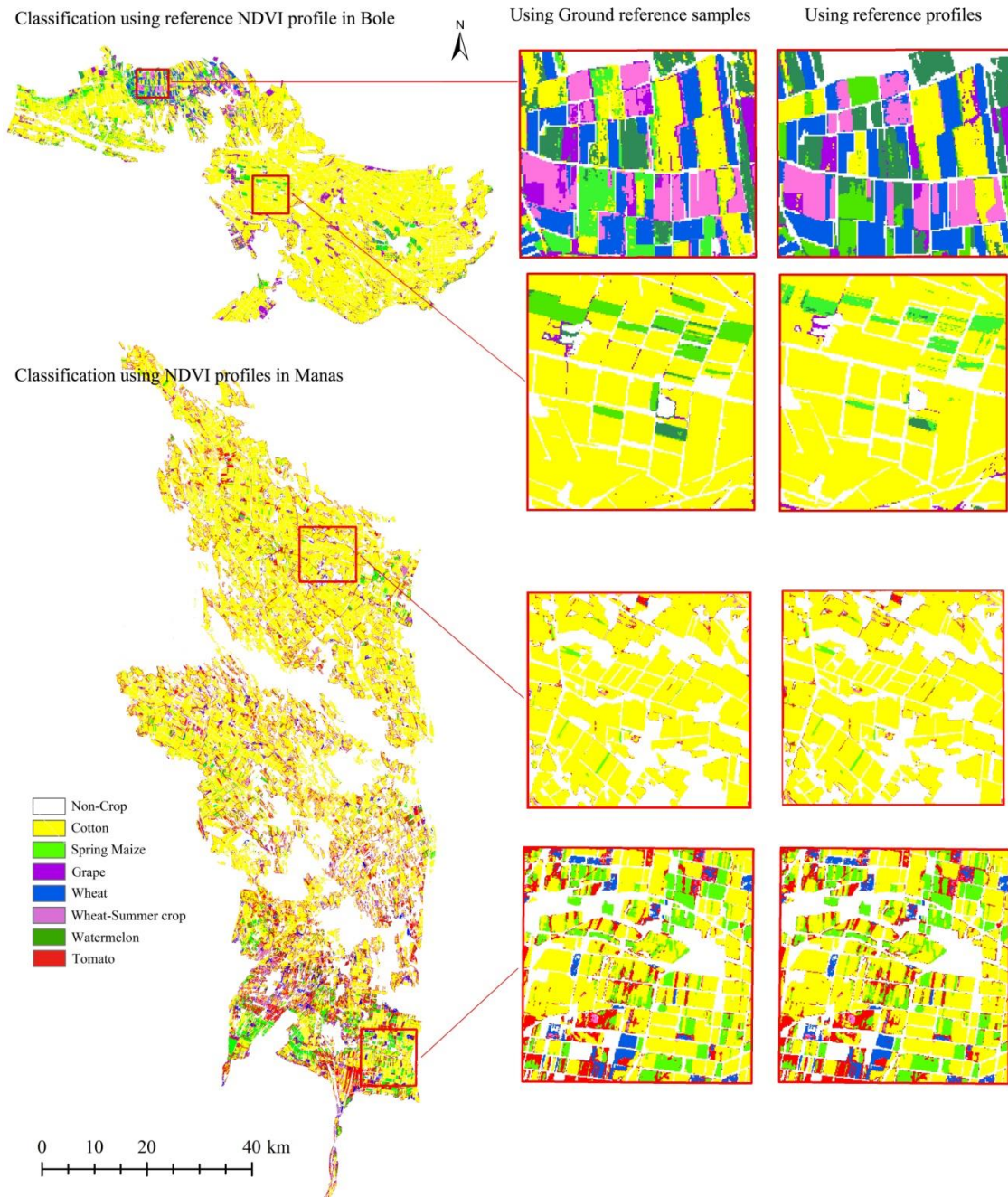


Figure 9. Crop map of Bole and Manas.

5. Discussion

This study uses the knowledge acquired from historical ground reference data and MODIS image time series to replace the ground reference in the classification year and classify the crops at 30 m resolution. The separability tests (JM distance) of the reference NDVI time series have shown that the crops in the study area are separable (Table 7). But the challenges of using the reference NDVI time series to identify crops at 30 m resolution contain the following three aspects: (1) the observation frequency of high resolution sensors; (2) the variation of the phenological metrics may result in the situation that the reference profiles cannot identify the crops in the classification year; and (3) the NDVI transformation (using linear relation to transform MODIS to Landsat/HJ NDVI) may attribute to some uncertainty in crop identification.

5.1. The Combination of Landsat and HJ Images

The reference NDVI profiles in this study are obtained from the MODIS 16-day composite NDVI product, and the reference profiles have shown the potential to separate the crops in the study area. However, for the images time series at 30 m spatial resolution, the first challenge is the temporal resolution of the image time series. Previous studies have indicated that some optimal time periods could classify the crop types with high accuracy and using more images provide little further improvement for the crop identification [35,55,56]. For the images from a single sensor at 30 m resolution, such as Landsat, the possibility of acquiring cloud-free images in each season is limited to only about 50% during winter and fall, and 60% during summer and spring on average [57]. Apparently, this relatively low image acquiring frequency cannot fulfill the requirement of the crop classification. In this study, we combined Landsat and HJ images and obtained the image time series of nearly 15-day temporal resolution. The combined images time series could classify the crops with high accuracy (the overall accuracy of using ground reference to classify crops is found in Tables 8 and 9), which is also consistent with other studies that the combination use of the images from multi-sensor could benefit the crop classification procedure, especially in large areas [58].

5.2. The Influence of Crop Growth Situation Variation on Crop Identification

Another challenge for crop identification using reference knowledge is the inter-annual phenological changes of the crops caused by the variation of temperature and precipitation among multiple years [43,59–61]. The temporal patterns of NDVI (Figure 10) have shown inter-annual variation in Bole and Manas. The NDVI time series of cotton among the five years are similar generally, except for slight variations during DOY 225~300. For spring maize, the NDVI peak of the profiles in all years are similar, the inter-annual variations are mainly in spring (DOY 100~150) and autumn (DOY 225~300). Grape and wheat have greater inter-annual variation, the NDVI of grape in 2007 is significantly higher during the entire growing season, and the wheat profiles showed that both greenup and NDVI-peak phases are 20 days earlier in 2007 than in the other years. In addition, NDVI peaks also vary by 0.06 and 0.11 for grape and wheat, respectively.

When using historical data of a single year as reference knowledge, the classification accuracies vary significantly. If the crop conditions of the reference year and the classification year are similar, the reference knowledge could achieve acceptable accuracy (such as using reference data of 2010 in Bole, Table 8). Otherwise, the reference knowledge and the NDVI pattern of the classification year are mismatched, and the classification accuracies are low (such as using reference data of 2007 in Manas, Table 9). Some complex methods have been proposed to use the shape of the NDVI profiles to measure the similarity [62]; but the shape of the NDVI time series sometimes changes because of the inter-annual phenological variation [43], which may lead to the failure of the shape-based similarity measures. Note that historical NDVI series from multiple years are used in this study, and reference knowledge from multiple years contains more growing conditions of the same crop and improves the classification performance when compared with the reference knowledge from a single year (Tables 8

and 9). However, there is a limitation: if the crop condition has not been recorded in the reference knowledge, this method may fail to correctly identify crops. Therefore, we need to collect as much historical reference data as possible to enrich the knowledge of reference NDVI time series.

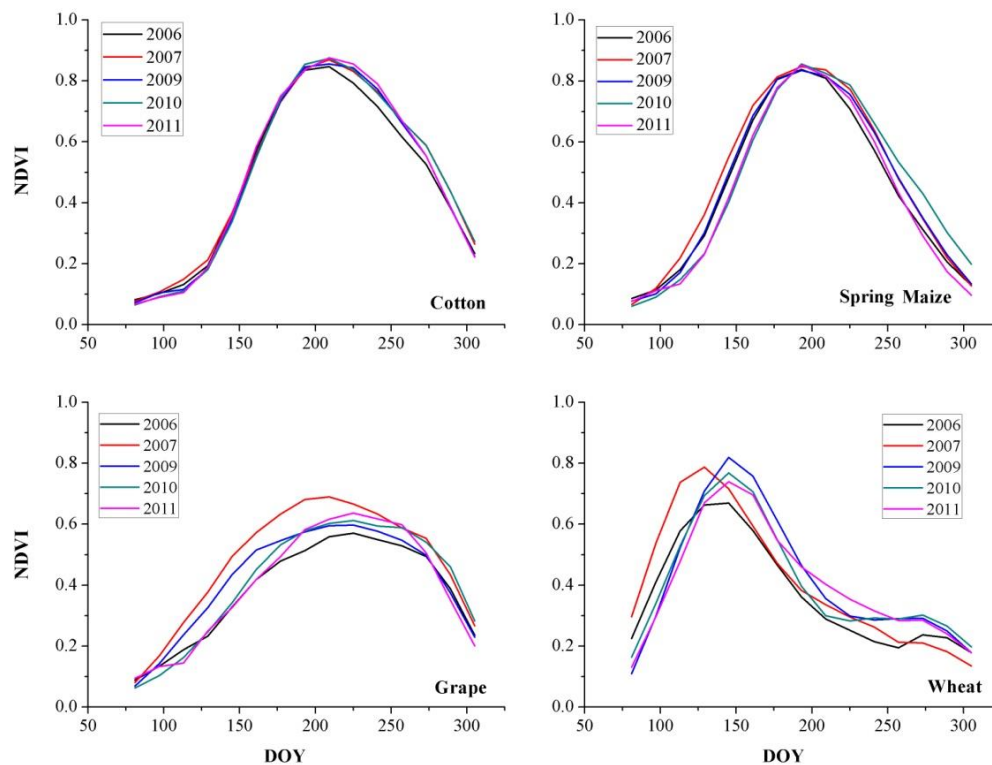


Figure 10. Comparison of inter-annual variation of historical MODIS NDVI time series averaged in Bole and Manas.

We select ABNet in this study because maybe the principle of ABNet is suitable for the acquisition of reference NDVI time series. The NDVI profiles of all samples among multiple years are used to derive the antibodies. Thus, each antibody could represent a specific phenological condition of one crop. Therefore, different distinctive patterns of the same crop are recorded by ABNet. Additionally, another advantage of ABNet is that it is an adaptive classifier, which needs no user-defined parameters during the training procedure.

5.3. The Influence of NDVI Transformation

In this study, we used MODIS NDVI time series as a reference, and transformed the MODIS NDVI to Landsat/HJ NDVI using linear relations. Thus, we do not need to take the radiation difference between Landsat and HJ into consideration [37]. Additionally, it is important to find the homogeneous area because the linear relations are calculated between the NDVI at different spatial resolution. Moreover, the samples used to fit the linear model need to be stratified distributed in the NDVI range for each time phase. Otherwise, the NDVI of the small sample number interval will be misestimated after the NDVI transformation. In our study area, the crop fields are characterized by homogenous; and generally, the transformed reference NDVI time series and the NDVI profile at 30 m resolution are matched (Figures 11 and 12). However, in some other study areas with disconnected patches, the lower “purity” of the MODIS pixels might have negative influence on the NDVI transformation. Thus, the transformed reference NDVI profile and the high resolution NDVI time series are mismatched, and classification accuracy is reduced.

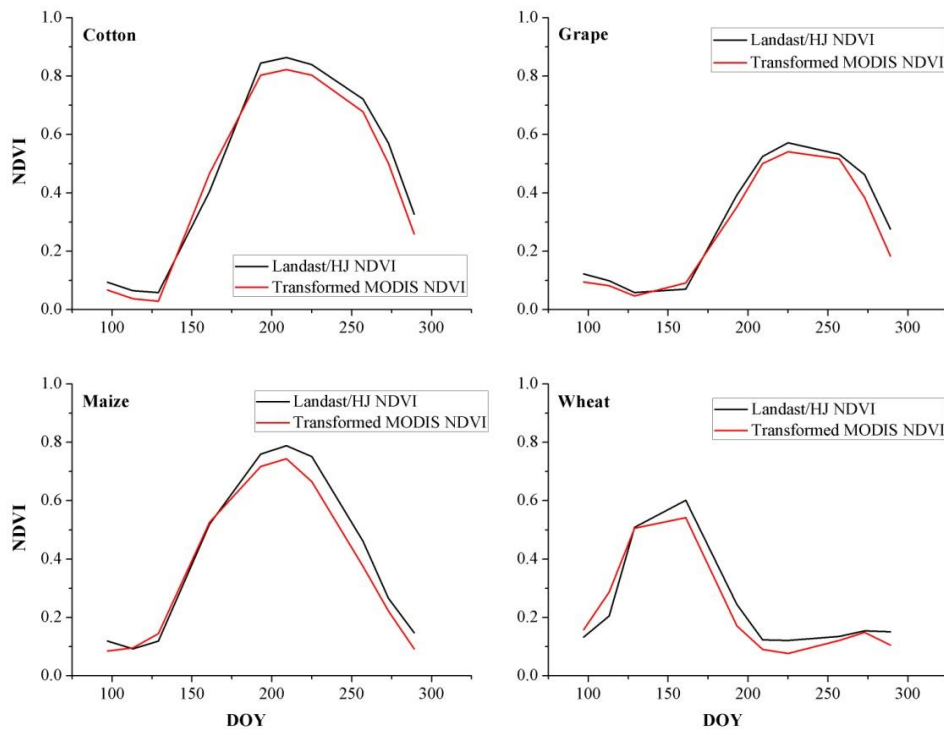


Figure 11. Transformed MODISNDVI and Landsat/HJ NDVI time series in Bole.

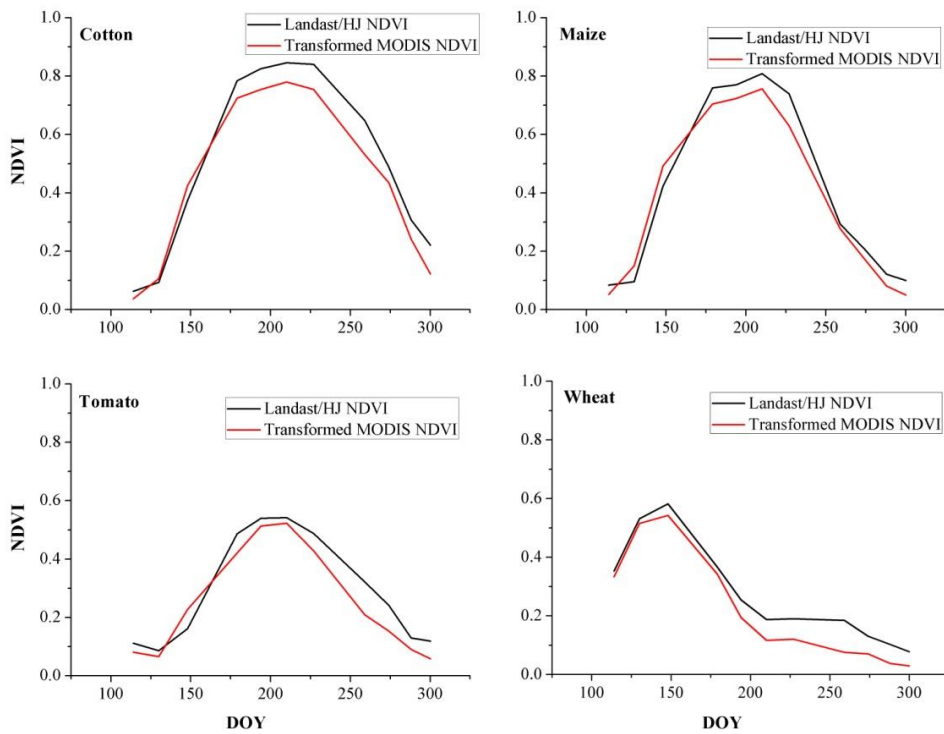


Figure 12. Transformed MODISNDVI and Landsat/HJ NDVI time series in Manas.

6. Conclusions

Most existing crop classification methods rely on ground-reference data from the same year, which have led to high labor and financial costs. In this study, we presented a crop classification method

using the historical NDVI time series of multiple years (from 2006 to 2010) to classify crop at 30 m resolution. The main conclusions are as follows.

- (1) The method proposed in this study could identify the dominant crops in the study areas, as the overall classification accuracies were 87.13% and 83.48% in Bole and Manas, respectively. Notably, no ground-reference data of the classification year were required in the classification process.
- (2) Reference NDVI time series obtained by historical NDVI profiles of multiple years could achieve higher accuracy than that from a single year. This is because there are phenological inter-annual variations among different years, and the reference NDVI profiles obtained from multiple years could contain more crop conditions and showed better classification performance.
- (3) The combination of Landsat and HJ data could increase the acquisition frequency of the 30 m image time series to 15-day, which is similar to the temporal resolution of the reference NDVI profiles. Moreover, the reference NDVI was transformed to Landsat/HJ NDVI; thus, we do not need to consider the radiation difference between Landsat and HJ images.

The limitation of this method is that we have to find homogenous areas that could contain pure MODIS pixels when transforming MODIS NDVI to Landsat/HJ NDVI. Therefore, the classification accuracy might be affected in some heterogeneous area. Additionally, the historical NDVI profiles should be collected as much as possible to enrich the knowledge of the reference NDVI time series. Generally, the method proposed in this study could be used to identify crop types at 30 m resolution when the ground reference data of the classification year is absent. As the results obtained depended on the specifics of the study area, other combinations of crop types and might have new problems. Therefore, further studies are essential to illustrate the feasibility of this approach in various study regions.

Acknowledgments: This work was supported by the National Natural Science Foundation of China (41371358, 41371416 and 41401399) and Natural Science Foundation of Heibei province (D2015207008). We thank all of the people working in the projects, especially for their efforts in the fieldwork.

Author Contributions: Pengyu Hao designed the experiments, processed the data and wrote the paper. Yulin Zhan, Li Wang and Zheng Niu contributed important ideas and considerations.

Conflicts of Interest: The authors declare no conflict of interest.

References

1. Kuenzer, C.; Knauer, K. Remote sensing of rice crop areas. *Int. J. Remote Sens.* **2013**, *34*, 2101–2139. [[CrossRef](#)]
2. Pan, Y.Z.; Li, L.; Zhang, J.S.; Liang, S.L.; Zhu, X.F.; Sulla-Menashe, D. Winter wheat area estimation from MODIS-EVI time series data using the Crop Proportion Phenology Index. *Remote Sens. Environ.* **2012**, *119*, 232–242. [[CrossRef](#)]
3. Hansen, M.C.; Egorov, A.; Potapov, P.V.; Stehman, S.V.; Tyukavina, A.; Turubanova, S.A.; Roy, D.P.; Goetz, S.J.; Loveland, T.R.; Ju, J.; *et al.* Monitoring conterminous United States (CONUS) land cover change with Web-Enabled Landsat Data (WELD). *Remote Sens. Environ.* **2014**, *140*, 466–484. [[CrossRef](#)]
4. Conrad, C.; Colditz, R.R.; Dech, S.; Klein, D.; Vlek, P.L.G. Temporal segmentation of MODIS time series for improving crop classification in Central Asian irrigation systems. *Int. J. Remote Sens.* **2011**, *32*, 8763–8778. [[CrossRef](#)]
5. Vieira, M.A.; Formaggio, A.R.; Renno, C.D.; Atzberger, C.; Aguiar, D.A.; Mello, M.P. Object based image analysis and data mining applied to a remotely sensed Landsat time-series to map sugarcane over large areas. *Remote Sens. Environ.* **2012**, *123*, 553–562. [[CrossRef](#)]
6. De Rainville, F.M.; Durand, A.; Fortin, F.A.; Tanguy, K.; Maldague, X.; Panneton, B.; Simard, M.J. Bayesian classification and unsupervised learning for isolating weeds in row crops. *Pattern Anal. Appl.* **2014**, *17*, 401–414. [[CrossRef](#)]
7. Howard, D.M.; Wylie, B.K. Annual crop type classification of the US great plains for 2000 to 2011. *Photogramm. Eng. Remote Sens.* **2014**, *80*, 537–549. [[CrossRef](#)]
8. Wu, Z.; Thenkabail, P.S.; Verdin, J.P. Automated cropland classification algorithm (ACCA) for California using multi-sensor remote sensing. *Photogramm. Eng. Remote Sens.* **2014**, *80*, 81–90. [[CrossRef](#)]

9. Thenkabail, P.S.; Wu, Z. An automated cropland classification algorithm (ACCA) for Tajikistan by combining Landsat, MODIS, and secondary data. *Remote Sens.* **2012**, *4*, 2890–2918. [[CrossRef](#)]
10. Han, W.; Yang, Z.; Di, L.; Mueller, R. Cropscape: A web service based application for exploring and disseminating us conterminous geospatial cropland data products for decision support. *Comput. Electron. Agric.* **2012**, *84*, 111–123. [[CrossRef](#)]
11. Conrad, C.; Rahmann, M.; Machwitz, M.; Stulina, G.; Paeth, H.; Dech, S. Satellite based calculation of spatially distributed crop water requirements for cotton and wheat cultivation in Fergana Valley, Uzbekistan. *Glob. Planet Chang.* **2013**, *110*, 88–98. [[CrossRef](#)]
12. Xiao, Y.; Mignolet, C.; Mari, J.F.; Benoit, M. Modeling the spatial distribution of crop sequences at a large regional scale using land-cover survey data: A case from France. *Comput. Electron. Agric.* **2014**, *102*, 51–63. [[CrossRef](#)]
13. Beziat, P.; Rivalland, V.; Tallec, T.; Jarosz, N.; Boulet, G.; Gentine, P.; Ceschia, E. Evaluation of a simple approach for crop evapotranspiration partitioning and analysis of the water budget distribution for several crop species. *Agric. For. Meteorol.* **2013**, *177*, 46–56. [[CrossRef](#)]
14. Zheng, B.; Myint, S.W.; Thenkabail, P.S.; Aggarwal, R.M. A support vector machine to identify irrigated crop types using time-series Landsat NDVI data. *Int. J. Appl. Earth Obs. Geoinform.* **2015**, *34*, 103–112. [[CrossRef](#)]
15. Fan, C.; Zheng, B.; Myint, S.W.; Aggarwal, R. Characterizing changes in cropping patterns using sequential Landsat imagery: An adaptive threshold approach and application to Phoenix, Arizona. *Int. J. Remote Sens.* **2014**, *35*, 7263–7278. [[CrossRef](#)]
16. Zhang, J.H.; Feng, L.L.; Yao, F.M. Improved maize cultivated area estimation over a large scale combining MODIS-EVI time series data and crop phenological information. *ISPRS J. Photogramm. Remote Sens.* **2014**, *94*, 102–113. [[CrossRef](#)]
17. Low, F.; Michel, U.; Dech, S.; Conrad, C. Impact of feature selection on the accuracy and spatial uncertainty of per-field crop classification using support vector machines. *ISPRS J. Photogramm. Remote Sens.* **2013**, *85*, 102–119. [[CrossRef](#)]
18. Zhong, L.H.; Gong, P.; Biging, G.S. Phenology-based crop classification algorithm and its implications on agricultural water use assessments in California's Central Valley. *Photogramm. Eng. Remote Sens.* **2012**, *78*, 799–813. [[CrossRef](#)]
19. Gallego, J.; Craig, M.; Michaelsen, J.; Bossyns, B.; Fritz, S. *Best Practices for Crop Area Estimation with Remote Sensing*; European Commission: Brussels, Luxembourg, 2008.
20. Zhong, L.H.; Hawkins, T.; Biging, G.; Gong, P. A phenology-based approach to map crop types in the San Joaquin Valley, California. *Int. J. Remote Sens.* **2011**, *32*, 7777–7804. [[CrossRef](#)]
21. Brown, J.C.; Kastens, J.H.; Coutinho, A.C.; Victoria, D.D.; Bishop, C.R. Classifying multiyear agricultural land use data from Mato Grosso using time-series MODIS vegetation index data. *Remote Sens. Environ.* **2013**, *130*, 39–50. [[CrossRef](#)]
22. Zhong, L.H.; Gong, P.; Biging, G.S. Efficient corn and soybean mapping with temporal extend ability: A multi-year experiment using Landsat imagery. *Remote Sens. Environ.* **2014**, *140*, 1–13. [[CrossRef](#)]
23. Foerster, S.; Kaden, K.; Foerster, M.; Itzerott, S. Crop type mapping using spectral-temporal profiles and phenological information. *Comput. Electron. Agric.* **2012**, *89*, 30–40. [[CrossRef](#)]
24. Rouse, J.W.; Haas, R.H.; Schell, J.A.; Deering, D.W.; Harlan, J.C. *Monitoring the Vernal Advancements and Retrogradation of Natural Vegetation*; National Aeronautics and Space Administration (NASA): Washington, DC, USA, 1974.
25. Huete, A.; Didan, K.; Miura, T.; Rodriguez, E.P.; Gao, X.; Ferreira, L.G. Overview of the radiometric and biophysical performance of the MODIS vegetation indices. *Remote Sens. Environ.* **2002**, *83*, 195–213. [[CrossRef](#)]
26. Wardlow, B.D.; Egbert, S.L. Large-area crop mapping using time-series MODIS 250 m NDVI data: An assessment for the U.S. Central Great Plains. *Remote Sens. Environ.* **2008**, *112*, 1096–1116. [[CrossRef](#)]
27. Wardlow, B.D.; Egbert, S.L.; Kastens, J.H. Analysis of time-series MODIS 250 m vegetation index data for crop classification in the us central great plains. *Remote Sens. Environ.* **2007**, *108*, 290–310. [[CrossRef](#)]
28. Sibanda, M.; Murwira, A. The use of multi-temporal MODIS images with ground data to distinguish cotton from maize and sorghum fields in smallholder agricultural landscapes of Southern Africa. *Int. J. Remote Sens.* **2012**, *33*, 4841–4855. [[CrossRef](#)]

29. Arvor, D.; Jonathan, M.; Meirelles, M.S.P.; Dubreuil, V.; Durieux, L. Classification of MODIS EVI time series for crop mapping in the state of Mato Grosso, Brazil. *Int. J. Remote Sens.* **2011**, *32*, 7847–7871. [[CrossRef](#)]
30. Lobell, D.B.; Asner, G.P. Cropland distributions from temporal unmixing of MODIS data. *Remote Sens. Environ.* **2004**, *93*, 412–422. [[CrossRef](#)]
31. Quarmby, N.A.; Townshend, J.R.G.; Settle, J.J.; White, K.H.; Milnes, M.; Hindle, T.L.; Silleos, N. Linear mixture modeling applied to AVHRR data for crop area estimation. *Int. J. Remote Sens.* **1992**, *13*, 415–425. [[CrossRef](#)]
32. Chang, J.; Hansen, M.C.; Pittman, K.; Carroll, M.; DiMiceli, C. Corn and soybean mapping in the United States using modn time-series data sets. *Agron. J.* **2007**, *99*, 1654–1664. [[CrossRef](#)]
33. Atzberger, C.; Rembold, F. Mapping the spatial distribution of winter crops at sub-pixel level using AVHRR NDVI time series and neural nets. *Remote Sens.* **2013**, *5*, 1335–1354. [[CrossRef](#)]
34. Lisita, A.; Sano, E.E.; Durieux, L. Identifying potential areas of cannabis sativa plantations using object-based image analysis of spot-5 satellite data. *Int. J. Remote Sens.* **2013**, *34*, 5409–5428. [[CrossRef](#)]
35. Hao, P.; Wang, L.; Niu, Z.; Aablikim, A.; Huang, N.; Xu, S.; Chen, F. The potential of time series merged from Landsat-5 TM and HJ-1 CCD for crop classification: A case study for Bole and Manas counties in Xinjiang, China. *Remote Sens.* **2014**, *6*, 7610–7631. [[CrossRef](#)]
36. De Wit, A.J.W.; Clevers, J.G.P.W. Efficiency and accuracy of per-field classification for operational crop mapping. *Int. J. Remote Sens.* **2004**, *25*, 4091–4112. [[CrossRef](#)]
37. Huang, W.J.; Huang, J.F.; Wang, X.Z.; Wang, F.M.; Shi, J.J. Comparability of red/near-infrared reflectance and NDVI based on the spectral response function between MODIS and 30 other satellite sensors using rice canopy spectra. *Sensors* **2013**, *13*, 16023–16050. [[CrossRef](#)] [[PubMed](#)]
38. LPDAAC. Vegetation Indices 16-Day 13 Global 250 m. Available online: https://lpdaac.usgs.gov/dataset_discovery/modis/modis_products_table/mod13q1 (accessed on 23 June 2015).
39. Chander, G.; Markham, B.L.; Helder, D.L. Summary of current radiometric calibration coefficients for Landsat MSS, TM, ETM+, and Eo-1 ALI sensors. *Remote Sens. Environ.* **2009**, *113*, 893–903. [[CrossRef](#)]
40. CRESDA GaoFen (GF-1) Satellite. Available online: <http://www.cresda.com/n16/n1130/n188475/188494.html> (accessed on 11 May 2016).
41. Vanonckelen, S.; Lhermitte, S.; Van Rompaey, A. The effect of atmospheric and topographic correction methods on land cover classification accuracy. *Int. J. Appl. Earth Obs. Geoinform.* **2013**, *24*, 9–21. [[CrossRef](#)]
42. Zhong, Y.; Zhang, L. An adaptive artificial immune network for supervised classification of multi-/hyperspectral remote sensing imagery. *IEEE Trans. Geosci. Remote Sens.* **2012**, *50*, 894–909. [[CrossRef](#)]
43. Lhermitte, S.; Verbesselt, J.; Verstraeten, W.W.; Coppin, P. A comparison of time series similarity measures for classification and change detection of ecosystem dynamics. *Remote Sens. Environ.* **2011**, *115*, 3129–3152. [[CrossRef](#)]
44. Kruse, F.A.; Lefkoff, A.B.; Boardman, J.W.; Heidebrecht, K.B.; Shapiro, A.T.; Barloon, P.J.; Goetz, A.F.H. The spectral image-processing system (sips)—Interactive visualization and analysis of imaging spectrometer data. *Remote Sens. Environ.* **1993**, *44*, 145–163. [[CrossRef](#)]
45. Murakami, T.; Ogawa, S.; Ishitsuka, N.; Kumagai, K.; Saito, G. Crop discrimination with multi-temporal SPOT/HRV data in the saga plains, Japan. *Int. J. Remote Sens.* **2001**, *22*, 1335–1348. [[CrossRef](#)]
46. Adam, E.; Mutanga, O. Spectral discrimination of papyrus vegetation (*Cyperus papyrus* L.) in swamp wetlands using field spectrometry. *ISPRS J. Photogramm. Remote Sens.* **2009**, *64*, 612–620. [[CrossRef](#)]
47. Huang, N.; He, J.S.; Niu, Z. Estimating the spatial pattern of soil respiration in Tibetan alpine grasslands using Landsat TM images and MODIS data. *Ecol. Indic.* **2013**, *26*, 117–125. [[CrossRef](#)]
48. Gao, F.; Masek, J.G.; Wolfe, R.E.; Huang, C. Building a consistent medium resolution satellite data set using moderate resolution imaging spectroradiometer products as reference. *J. Appl. Remote Sens.* **2010**, *4*. [[CrossRef](#)]
49. Gong, P.; Wang, J.; Yu, L.; Zhao, Y.C.; Zhao, Y.Y.; Liang, L.; Niu, Z.G.; Huang, X.M.; Fu, H.H.; Liu, S.; *et al.* Finer resolution observation and monitoring of global land cover: First mapping results with Landsat TM and ETM + data. *Int. J. Remote Sens.* **2013**, *34*, 2607–2654. [[CrossRef](#)]
50. Hawthorne, B. Hawth’s Analysis Tools for Arcgis. Available online: <http://www.spatial ecology.com/htools/overview.php> (accessed on 30 January 2016).

51. Conrad, C.; Dech, S.; Dubovyk, O.; Fritsch, S.; Klein, D.; Low, F.; Schorcht, G.; Zeidler, J. Derivation of temporal windows for accurate crop discrimination in heterogeneous croplands of Uzbekistan using multi-temporal rapid-eye images. *Comput. Electron. Agric.* **2014**, *103*, 63–74. [[CrossRef](#)]
52. Forkuor, G.; Conrad, C.; Thiel, M.; Ullmann, T.; Zoungrana, E. Integration of optical and Synthetic Aperture Radar imagery for improving crop mapping in northwestern Benin, West Africa. *Remote Sens.* **2014**, *6*, 6472–6499. [[CrossRef](#)]
53. Congalton, R.G. A review of assessing the accuracy of classifications of remotely sensed data. *Remote Sens. Environ.* **1991**, *37*, 35–46. [[CrossRef](#)]
54. Story, M.; Congalton, R.G. Accuracy assessment—A users perspective. *Photogramm. Eng. Remote Sens.* **1986**, *52*, 397–399.
55. Van Niel, T.G.; McVicar, T.R. Determining temporal windows for crop discrimination with Remote Sensing: A case study in south-eastern Australia. *Comput. Electron. Agric.* **2004**, *45*, 91–108. [[CrossRef](#)]
56. Jia, K.; Wu, B.; Li, Q. Crop classification using HJ satellite multispectral data in the North China Plain. *J. Appl. Remote Sens.* **2013**, *7*. [[CrossRef](#)]
57. Ju, J.C.; Roy, D.P. The availability of cloud-free Landsat ETM plus data over the conterminous united states and globally. *Remote Sens. Environ.* **2008**, *112*, 1196–1211. [[CrossRef](#)]
58. USDA. National Agricultural Statistics Service. Available online: <http://www.nass.usda.gov/research/Cropland/SARS1a.htm> (accessed on 11 May 2016).
59. Zhang, X.Y. Reconstruction of a complete global time series of daily vegetation index trajectory from long-term AVHRR data. *Remote Sens. Environ.* **2015**, *156*, 457–472. [[CrossRef](#)]
60. Melaas, E.K.; Friedl, M.A.; Zhu, Z. Detecting interannual variation in deciduous broadleaf forest phenology using Landsat TM/ETM plus data. *Remote Sens. Environ.* **2013**, *132*, 176–185. [[CrossRef](#)]
61. Zhang, X.Y.; Tan, B.; Yu, Y.Y. Interannual variations and trends in global land surface phenology derived from enhanced vegetation index during 1982–2010. *Int. J. Biometeorol.* **2014**, *58*, 547–564. [[CrossRef](#)] [[PubMed](#)]
62. Evans, J.P.; Geerken, R. Classifying rangeland vegetation type and coverage using a Fourier component based similarity measure. *Remote Sens. Environ.* **2006**, *105*, 1–8. [[CrossRef](#)]



© 2016 by the authors; licensee MDPI, Basel, Switzerland. This article is an open access article distributed under the terms and conditions of the Creative Commons Attribution (CC-BY) license (<http://creativecommons.org/licenses/by/4.0/>).